J Mater Sci (2013) 48:1035–1041
DOI 10.1007/s10853-012-6835-y

Effects of MnO_2 and sintering temperature on microstructure, ferroelectric, and piezoelectric properties of $Ba_{0.85}Ca_{0.15}Ti_{0.90}Zr_{0.10}O_3$ lead-free ceramics

Meng Jiang · Qin Lin · Dunmin Lin · Qiaoji Zheng · Ximing Fan · Xiaochun Wu · Hailing Sun · Yang Wan · Lang Wu

Received: 26 April 2012 / Accepted: 24 August 2012 / Published online: 6 September 2012

Abstract $Ba_{0.85}Ca_{0.15}Ti_{0.90}Zr_{0.10}O_3 + x$mol% MnO_2 lead-free ceramics have been prepared by a conventional sintering method and the effects of MnO_2 and sintering temperature on microstructure, ferroelectric, and piezoelectric properties of $Ba_{0.85}Ca_{0.15}Ti_{0.90}Zr_{0.10}O_3$ lead-free ceramics have been studied. The addition of 0.25 mol% MnO_2 promotes grain growth, improves the ferroelectricity of the ceramics and strengthens ferroelectric tetragonal–ferroelectric orthorhombic phase transition near 40 °C. Because of the coexistence of tetragonal and orthorhombic phases and the combinatory effects of soft and hard doping of Mn ions, the ceramic with $x = 0.25$ exhibits the optimum piezoelectric properties ($d_{33} = 306$ pC/N and $k_p = 42.2$ %, respectively). Excess MnO_2 inhibits the grain growth and degrades the ferroelectric and piezoelectric properties of the ceramics. Sintering temperature has an important influence on the microstructure, tetragonal–orthorhombic phase transition near 40 °C, ferroelectric and piezoelectric properties of the ceramics. The increase in sintering temperature leads to large grains and more noticeable tetragonal–orthorhombic phase transition near 40 °C, enhances ferroelectricity and thus improves effectively the piezoelectricity of the ceramics. The $Ba_{0.85}Ca_{0.15}Ti_{0.90}Zr_{0.10}O_3$ ceramic sintered at 1350 °C possesses the optimum piezoelectric constant d_{33} value of 373 pC/N.

M. Jiang · Q. Lin · D. Lin (✉) · Q. Zheng (✉) · X. Fan · X. Wu · H. Sun · Y. Wan
College of Chemistry and Materials Science, and Visual Computing and Virtual Reality Key Laboratory of Sichuan Province, Sichuan Normal University, Chengdu 610066, China
e-mail: ddmd222@yahoo.com.cn

Q. Zheng
e-mail: joyce@sicnu.edu.cn

L. Wu
State Key Laboratory Cultivation Base for Nonmetal Composites and Functional Materials, Southwest University of Science and Technology, Mianyang 621010, China

Introduction

Lead-based piezoelectric ceramics with perovskite structure have been widely used in sensors, actuators as well as microelectronic devices due to their superior piezoelectric properties. However, the use of lead-based ceramics has caused serious environmental problems because of the high toxicity of lead oxide. Therefore, it is necessary to develop lead-free piezoelectric ceramics.

Barium titanate ($BaTiO_3$) is a classic perovskite ferroelectric with tetragonal symmetry at room temperature. Zr^{4+}- and Sn^{4+}-modified $BaTiO_3$ materials have been extensively investigated for dielectric applications [1, 2]. Compared with $Pb(Zr,Ti)O_3$-based perovskite ceramics ($d_{33} = 289$–710 pC/N) [3], pure $BaTiO_3$ possesses relatively poor piezoelectricity ($d_{33} = 191$ pC/N) [4]. Therefore, $BaTiO_3$-based materials are widely used as dielectric materials but not piezoelectrics. However, recently, Liu and Ren [5] designed a ferroelectric system $0.5Ba(Zr_{0.2}Ti_{0.8})O_3$–$0.5(Ba_{0.7}Ca_{0.3})TiO_3$ with a super high d_{33} ($\sim$620 pC/N) and reported the origination of the high piezoelectricity from a TCP (tricritical point)-type MPB (morphotropic phase boundary). Since then, as one of promising candidates for lead-free piezoelectric materials, $BaTiO_3$-based ceramics have attracted considerable attention. Many modified $BaTiO_3$-based lead-free piezoelectric ceramics (e.g., $(Ba_{1-x}Ca_x)(Ti_{0.98}Zr_{0.02})O_3$ [6], $(Ba_{0.95}Ca_{0.05})(Ti_{1-x}Zr_x)O_3$ [7], ZnO-doped $Ba_{0.85}Ca_{0.15}Ti_{0.90}Zr_{0.10}O_3$ [8], $(Ba_{0.93}Ca_{0.07})(Ti_{0.95}Zr_{0.05})O_3$ [9], etc.) have been prepared and the effects of sintering temperature [10], dwell time during sintering [11], and poling conditions [12] on the piezoelectric

properties of $Ba_{0.85}Ca_{0.15}Ti_{0.90}Zr_{0.10}O_3$ ceramics have been investigated. As known, for Pb(Zr,Ti)O_3-based ceramics, the doping of metal oxides (e.g., La_2O_3, Nb_2O_5, MnO_2, Fe_2O_3, etc.) is an effective approach to improve the electrical properties of the ceramics. Amongst the metal oxide dopants, MnO_2 is the most interesting because of the multi-valence states (Mn^{2+}, Mn^{3+}, and Mn^{4+}) of Mn ions [13, 14] and has been extensively used to substitute the A- or/and B-site ions of ferroelectrics for tailoring electrical properties[13–20]. It has been found that low level doping of MnO_2 leads to "soft" and "hard" effects simultaneously and thus induce the increase in piezoelectricity (d_{33} and k_p) and relative permittivity ε_r and the decrease in loss tangent tanδ in (Ca,Sr)$Bi_4Ti_4O_{15}$- [13], PZT- [14], BNT- [19], and (Sr,Ca)$NaNb_5O_{15}$-based [20] ceramics. However, there is little work on MnO_2 doping for 0.5Ba($Zr_{0.2}Ti_{0.8}$)–0.5($Ba_{0.7}Ca_{0.3}$)TiO_3 (i.e., $Ba_{0.85}Ca_{0.15}Ti_{0.90}Zr_{0.10}O_3$) ceramics. In this study, MnO_2-doped $Ba_{0.85}Ca_{0.15}Ti_{0.90}Zr_{0.10}O_3$ ceramics were prepared by an ordinary sintering method and the effects of MnO_2 on the microstructure, ferroelectric, and piezoelectric properties were studied. In addition, our previous study shows that the $Ba_{0.85}Ca_{0.15}Ti_{0.90}Zr_{0.10}O_3$ ceramic with large grains exhibits high piezoelectricity. Therefore, the possible relationship between electrical properties and grain size were briefly investigated by sintering the $Ba_{0.85}Ca_{0.15}Ti_{0.90}Zr_{0.10}O_3$ ceramic at different temperature.

Experimental

$Ba_{0.85}Ca_{0.15}Ti_{0.90}Zr_{0.10}O_3$ + $x$mol% MnO_2 (BCZT-Mn-x) ceramics were prepared by a conventional ceramic technology using metal oxides and carbonate powders: $BaCO_3$(99 %, Sinopharm Chemical Reagent Co., Ltd, China), $CaCO_3$(99 %, Sinopharm Chemical Reagent Co., Ltd, China), TiO_2(98 %, Sinopharm Chemical Reagent Co., Ltd, China), ZrO_2 (99 %, Sinopharm Chemical Reagent Co., Ltd, China), and MnO_2(97.5 %, Sinopharm Chemical Reagent Co., Ltd, China). The powders in the stoichiometric ratio of $Ba_{0.85}Ca_{0.15}Ti_{0.90}Zr_{0.10}O_3$ (BCTZ) were first mixed thoroughly in ethanol using zirconia balls for 10 h. After the calcination at 1100 °C for 4 h, MnO_2 powder was added. The mixture was ball-milled again for 10 h, mixed thoroughly with a poly(vinyl alcohol) binder solution and then pressed into disk samples. After removal of the binder, the samples were sintered at 1250–1350 °C for 2 h. The sintered ceramics were coated with silver paste to form electrodes on both sides and fired at 810 °C for 10 min. The ceramics were poled at room temperature for 40 min in a silicone oil bath under a dc filed of 3 kV/mm.

The crystalline structure of the sintered samples was determined using X-ray diffraction (XRD) analysis with CuKα radiation (DX1000, China). The microstructures were observed using scanning electron microscopy (JSM-5900LV, Japan). The relative permittivity ε_r at 1 kHz was measured as a function of temperature using an LCR meter (Agilent E4980A, USA). The polarization hysteresis (P–E) loops were measured using a ferroelectric measuring system (Premier II, Radiant Technologies, Inc., USA). The planar electromechanical coupling factor k_p was determined by the resonance method according to the IEEE Standards 176 using an impedance analyzer (Agilent 4294A, USA). The loss tangent tanδ at 1 kHz was measured using an impedance analyzer (Agilent 4294A, USA). The piezoelectric constant d_{33} was measured using a piezo-d_{33} meter (ZJ-6A, China).

Results and discussions

The XRD patterns of the BCZT-Mn-x ceramics are shown in Fig. 1. All the ceramics have a pure perovskite structure and no second phases were detected. The coexistence of orthorhombic and tetragonal phases near room temperature has been reported in $Ba_{0.85}Ca_{0.15}Ti_{0.90}Zr_{0.10}O_3$ ceramics [5]. The addition of MnO_2 has no obvious influence on the crystal structure of the BCTZ ceramics.

The SEM micrographs of the BCZT-Mn-x ceramics with $x = 0$, 0.25, 0.75, and 2.0 are shown in Fig. 2. All the ceramics have a dense microstructure. From Fig. 2a, for the ceramic with $x = 0$, only a few large grains (about 15 μm) are distributed in large numbers of small grains (about 3 μm) (Fig. 2a). As x increases to 0.25, an inhomogeneous grain size distribution can be observed. The grains of the ceramic with $x = 0.25$ exhibit an obvious bimodal grain size distribution and the big grains with an average size of

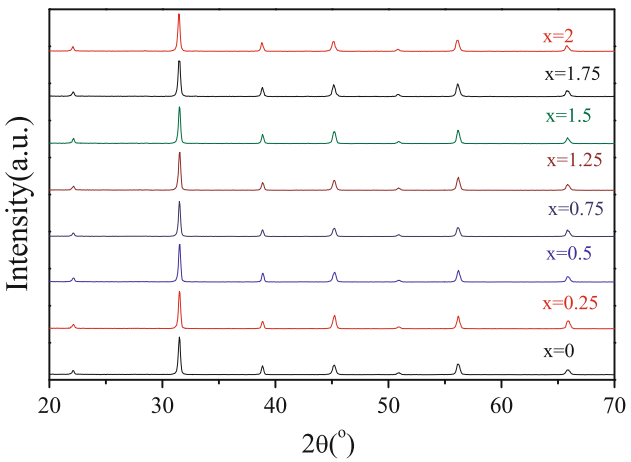

Fig. 1 XRD patterns of the BCZT-Mn-x ceramics

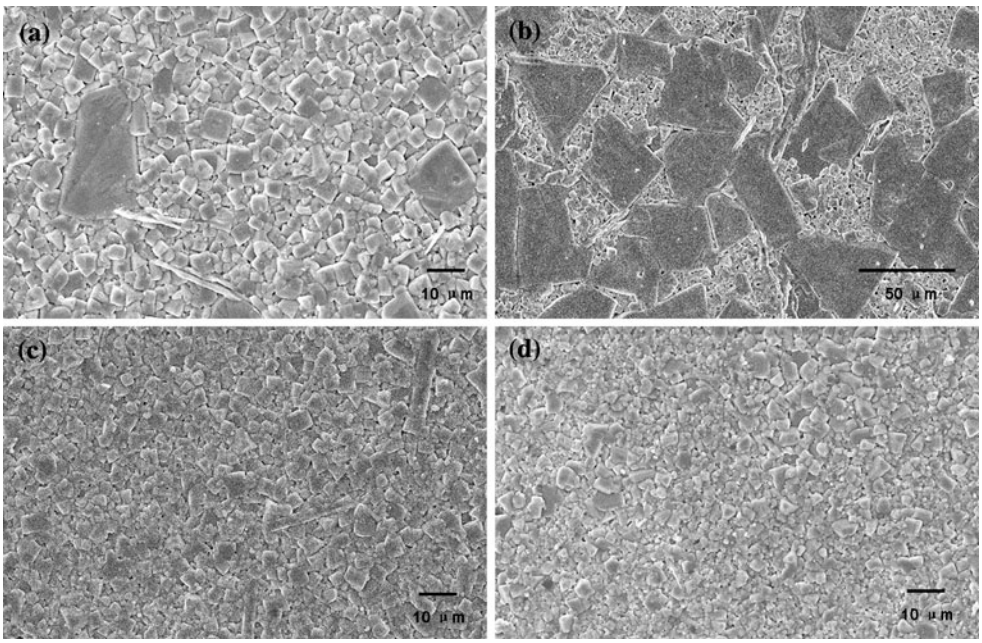

Fig. 2 SEM micrographs of the BCZT-Mn-x ceramics sintered at 1300 °C for 2 h: **a** $x = 0$, **b** $x = 0.25$, **c** $x = 0.75$, **d** $x = 2$

about 45 μm are surrounded by the small grains with an average size of 3.5 μm (Fig. 2b). However, as x further increases to 0.75 and 2.0, the grains become relatively uniform and much smaller. The average grain sizes for the ceramics with $x = 0.75$ and 2.0 are about 2.5 and 2.0 μm. Obviously, a small amount of MnO_2 can promote effectively the grain growth, while excess MnO_2 causes a significant inhibition of grain growth. Similar influence of MnO_2 on microstructure has been observed in PZT-based ceramics [15, 16]. For the BCTZ-Mn-x ceramics, a small amount of MnO_2 within the solubility limit of Mn ions can be dissolved in the perovskite structure and Mn ions substitute the B-site Ti^{4+} and Zr^{4+} of the ceramics to create oxygen vacancies. The oxygen vacancies increase the mobility of grain boundary and promote the mass transportation [15, 16]. As a result, the grain becomes large with x increasing. However, excess MnO_2 may accumulate near the grain boundaries [14], reduce their mobility and thus suppress the grain growth [15, 16].

Figure 3a shows the P–E loops of BCTZ-Mn-x ceramics, while the variations of the remanent polarization P_r and coercive field E_c of the BCTZ-Mn-x ceramics with x are shown in Fig. 3b. All the ceramics exhibit a typical P–E loop for ferroelectrics (Fig. 3a). From Fig. 3b, the observed P_r increases and then decrease with x increasing, giving the maximum value of 11.7 μC/cm^2 at $x = 0.25$. For the ceramics with $x \geq 0.75$, the observed P_r has a weak dependence on x and retains the small values of about 3–4 μC/cm^2. The observed E_c keeps nearly unchanged ($\sim$0.32 kV/mm) with x increasing to 0.75 and then increases to 0.55 kV/mm with x further increasing to 2.0. The large P_r in the ceramic with $x = 0.25$ may be attributed to the large grain size. Similar result has been observed in $BaTiO_3$ ferroelectric [21].

Figure 4 shows the temperature dependence of ε_r for the BCZT-Mn-x ceramics. All the BCTZ-Mn-x ceramics exhibit the paraelectric cubic-ferroelectric tetragonal phase transition peak at T_C. The ferroelectric tetragonal–ferroelectric orthorhombic phase transition near 40 (T_{O-T}) can be also observed, suggesting that orthorhombic and tetragonal phases coexist near room temperature in the BCTZ-Mn-x ceramics. As x increases from 0 to 0.25, the phase transition peaks at T_{O-T} and T_C becomes more noticeable. However, as x further increases, the transition peaks at T_{O-T} and T_C become gradually smeared. It has been found that for $K_{0.5}Na_{0.5}NbO_3$ [22], $BaTiO_3$ [23], and $PbTiO_3$ [24] ceramics, fine grain weakens the dielectric peak's sharpness and intensity and smears phase transition. Similarly, the weakness of the phase transitions at T_{O-T} and T_C of the BCTZ-Mn-x ceramics with $x \geq 0.5$ should be attributed to the small grain size as shown in Fig. 2c, d.

The variations of d_{33}, k_p, ε_r, and tanδ with x for the BCTZ-Mn-x ceramics are shown in Fig. 5. The observed d_{33}, k_p, and ε_r increase with x increasing and then decrease, giving the maximum values of 306 pC/N, 42.0 % and 3427 at $x = 0.25$, respectively. When $x \geq 0.75$, the observed d_{33}, k_p, and ε_r exhibit relatively weak dependence on x. The observed tanδ decreases with increasing x and then increases, reaching a minimum value of 1.0 % at $x = 0.75$.

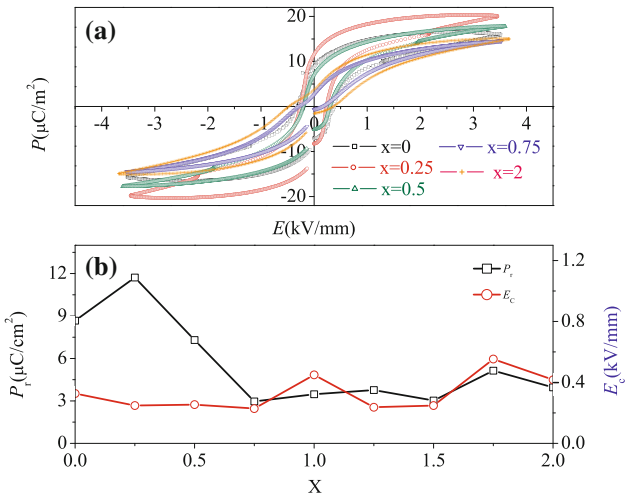

Fig. 3 **a** *P–E* hysteresis loops of the BCTZ-Mn-*x* ceramics: $x = 0$, 0.25, 0.5, 0.75, and 2. **b** Variations of P_r and E_c with *x* for the BCTZ-Mn-*x* ceramics

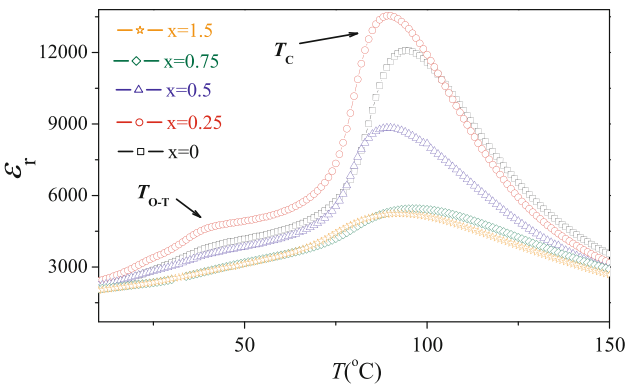

Fig. 4 Temperature dependence of ε_r for the BCTZ-Mn-*x* ceramics

It is known that a small amount of MnO_2 induces the combinatory effects of donor and acceptor doping in PZT-, $Bi_{0.5}Na_{0.5}TiO_3$−, and $(Ca_{1-x}Sr_x)Bi_4Ti_4O_{15}$-based ceramics [14–16]. At high temperature, Mn^{2+} (0.091 nm) and Mn^{3+} (0.07 nm) coexist [13, 14]. For the BCTZ-Mn-*x* ceramics with $x \leq 0.25$, Mn^{2+} and Mn^{3+} can enter the A-sites (Mn^{3+}: donor doping), causing the increase in the d_{33}, k_p, and ε_r. Simultaneously, part of Mn^{3+} ions enter the B-sites (acceptor doping), leading to the decrease in tanδ. As *x* increase above 0.25 mol %, the solubility limit of Mn ions in the A- and B-sites of the ceramics is reached. Excess Mn ions may accumulate near the grain boundaries and thus lead to the degradation of the d_{33}, k_p, ε_r, and tanδ.

From Figs. 2, 3, 4, 5, the BCTZ-Mn-0.25 ceramic with large grains possesses stronger ferroelectricity, more noticeable phase transition peaks at T_C and T_{O-T} and better piezoelectricity than the ceramics with small grains. Therefore, it may be inferred that the grain size of BCTZ-Mn-*x* ceramics has an important influence on the phase transition and

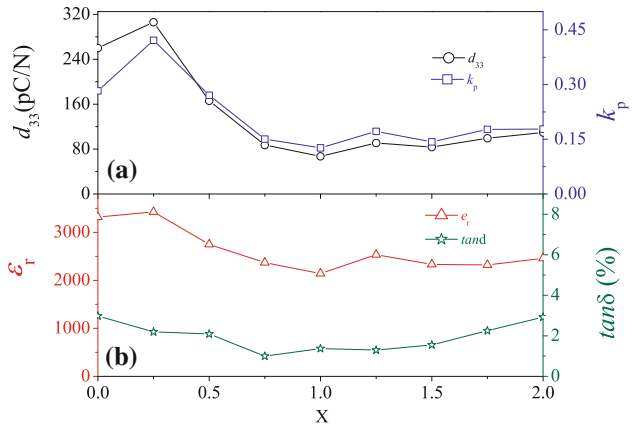

Fig. 5 **a** Piezoelectric properties and **b** dielectric properties of Mn-doped BCTZ ceramics as a function of *x*

electrical properties. To demonstrate the effects of grain size on phase transition and electrical properties of the BCTZ-Mn-*x* ceramics, a well-known $0.5Ba(Zr_{0.2}Ti_{0.8})$–$0.5(Ba_{0.7}Ca_{0.3})$-TiO_3 composition [5] (i.e., BCTZ, the BCTZ-Mn-0 ceramics without MnO_2 doping) was selected and sintered at different temperature. Figure 6 shows the SEM micrographs of the BCTZ ceramics at different sintering temperature T_s. The ceramic sintered at 1250 °C has a small average grain size of 3.8 μm (Fig. 6a). The evolution process of grain growth with T_s can be clearly observed: as T_s increases from 1250 to 1275 °C, the grains become slightly large and denser; when T_s increases to 1300 °C, a few large grains began to appear; with T_s increasing to 1325 °C, part of the grains began to growth up and the grains have a bimodal grain size distribution with large grains of diameters about 48 μm uniformly distributed among the grains which are of much smaller diameters, about 3.7 μm; and as T_s further increases to 1350 °C, the rest of small grains grow into large grains. The average grain sizes of the ceramics sintered at 1275, 1300, 1325, and 1350 °C for 2 h are about 4.2, 5.2, 28.4, and 33.0 μm, respectively.

The temperature dependences of ε_r for the BCTZ ceramics sintered at different T_s are shown in Fig. 7. As grain size increases, the phase transition peaks near 90 °C (T_C) becomes gradually sharper. It is also observed that the phase transition near 40 °C (T_{O-T}) gradually appears and becomes more noticeable. Obviously, the grain size has a significant influence on the phase transition characteristics of the BCTZ ceramics. Similar phenomena have been observed in $K_{0.5}Na_{0.5}NbO_3$, $BaTiO_3$, and $PbTiO_3$ ceramics [22–24].

The *P–E* loops of BCTZ ceramics sintered at different T_s are shown in Fig. 8a, while the variations of P_r and E_c of the BCTZ ceramics with T_s are shown in Fig. 8b. For the ceramic sintered at 1250 °C, a flattened and slanted loop is observed. As T_s (grain size) increases to 1350 °C, the loop becomes gradually saturated and square like. At

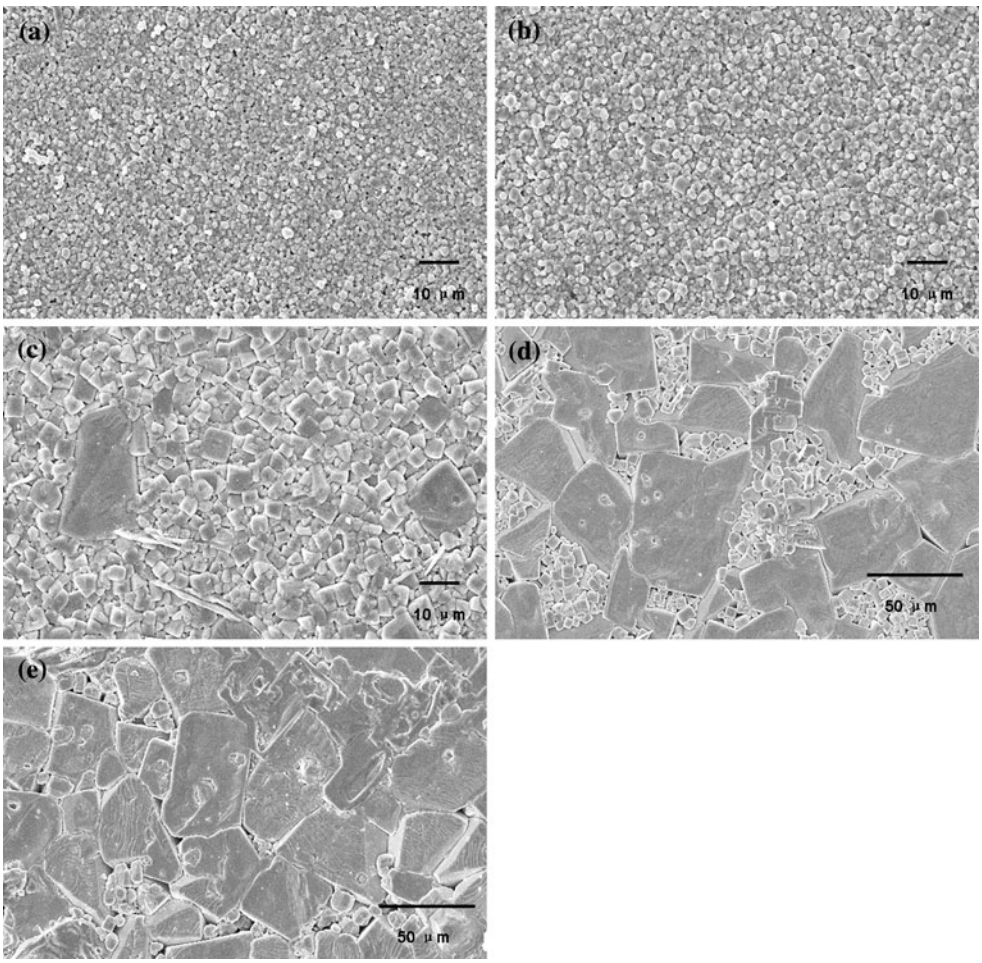

Fig. 6 SEM micrographs of the BCTZ ceramics at different sintering temperature T_s: **a** 1250 °C, **b** 1275 °C, **c** 1300 °C, **d** 1325 °C, and **e** 1350 °C

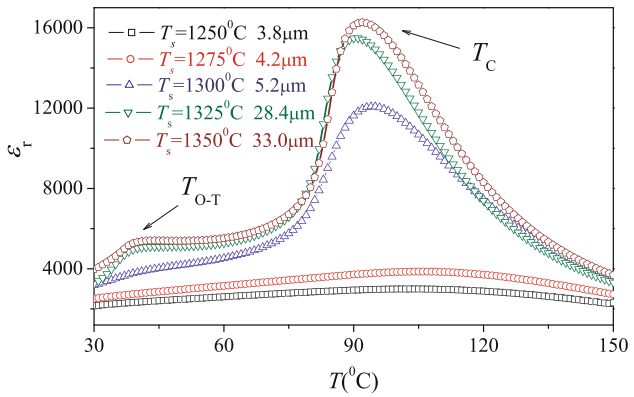

Fig. 7 Temperature dependences of ε_r for the BCTZ ceramics sintered at different T_s

$T_s = 1350$ °C, a large P_r (10.1 μC/cm^2) and a relatively low E_c (0.22 kV/mm) are obtained (Fig. 8a). From Fig. 8b, the observe P_r increases with T_s increasing, while the observed E_C decreases with T_s increasing. It can be noted that the ceramics with large grains exhibits larger P_r and lower E_C than the ceramics with small grains. This should be attributed to the easier polarization reversal process of ferroelectric domain in larger grains than in smaller grains [17, 21].

Figure 9 shows the variations of d_{33}, k_p, ε_r, tanδ, and grain size with T_s for the BCTZ ceramics. For the BCTZ ceramics sintered at $T_s < 1300$ °C, the observed d_{33} and k_p exhibit a weak dependence on T_s and give the relatively low values of about 30 pC/N and 11.0 %, respectively. However, as T_s further increases to 1350 °C, the observed d_{33} and k_p increase greatly to 373 pC/N and 53.0 %. The observed ε_r increases monotonously from 2159 to 3974 with T_s increasing from 1250 to 1350 °C. The observed tanδ increases and then decreases with T_s increasing, reaching a maximum value of 2.98 % at $T_s = 1300$.

It can be seen from Figs. 2, 3, 4, 5, 6, 7, 8, and 9 that grain size in the BCTZ ceramic is positively related with the coexistence of orthorhombic and tetragonal phases, ferroelectricity and piezoelectricity of the BCTZ ceramic; and the BCTZ ceramics with large grains possess much better

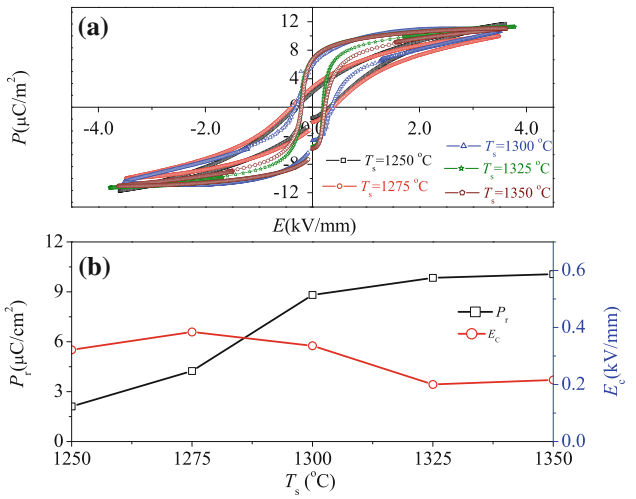

Fig. 8 **a** *P–E* hysteresis loops of the BCTZ ceramics sintered at different T_s, and **b** Variations of P_r and E_c of the BCTZ ceramics with T_s

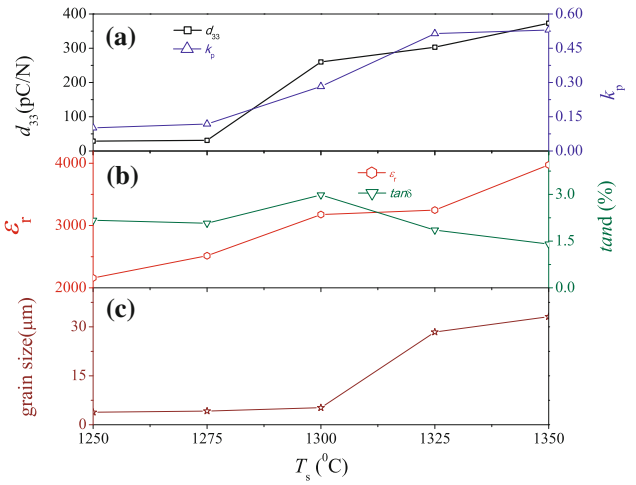

Fig. 9 Variations of d_{33}, k_p, ε_r, tanδ, and grain size with T_s for the BCTZ ceramics

ferroelectricity and piezoelectricity than those with small grains. It has been known that grain size has an important influence on the electrical properties of piezoelectric ceramics [22, 25–27]. From Figs. 2, 3, 4, 5, 6, 7, 8, and 9, well-saturated and square like *P–E* loops with large P_r are observed and good piezoelectricity is obtained in the ceramics with large grains, while the ceramics with small grains exhibit slanted and narrowed loops with small P_r and possess poor piezoelectricity. The internal mechanisms of the strong dependence of ferroelectric and piezoelectric properties on grain size may be attributed to the variation of domain structure with grain size [28–30]. In general, the correlation between gain size and domain size can be expressed [28, 29] as (Domain size) $\propto$ (grain size)^m, where m is related to the grain size. As grain size increases, domain size increases and domain boundary decreases [15]. This leads to the increase in the contribution to polarization switching and piezoelectric response from extrinsic effect (domain wall motion) [17] and thus larger polarization is obtained in the ceramics with large grains than in those with small grains, which causes the significant improvement in the piezoelectric and ferroelectric properties in the ceramics with large grains. Compared with the ceramics with large grains, the motion of domain walls in the ceramics with small grains is more difficult [30]. Therefore, it can be concluded that the increase in the domain size leads to a significant improvement in the ferroelectricity and piezoelectricity in the ceramics with large grains. On the other hand, according to the thermodynamic theory of ferroelectrics, the piezoelectric coefficient d_{33} can generally be expressed as a function of its relative permittivity ε_r and spontaneous polarization P_s [31]: $d_{33} = 2Q_{11}\varepsilon_0\varepsilon_r P_s$, where Q_{11} is the electrostrictive coefficient which is related to the domain structure and should not change significantly for perovskite materials. Accordingly, d_{33} is greatly dependent on ε_r and P_s. From Figs. 3, 5, 8, and 9, the ceramics with large grains possesses relatively large P_s and ε_r and thus exhibits the highest d_{33}. It should be also noted that the ceramics with large grains exhibit more noticeable tetragonal–orthorhombic phase transition than those with small grains. This clearer coexistence of tetragonal and orthorhombic phase also enhances the piezoelectricity of the ceramics with large grains. The effects of grain size on electrical properties and phase transitions in the BCTZ will be further studied systematically.

Conclusions

Lead-free ceramics $Ba_{0.85}Ca_{0.15}Ti_{0.90}Zr_{0.10}O_3 + x$mol % MnO_2 were prepared by an ordinary sintering technique and the effects of MnO_2 and sintering temperature on microstructure, phase transition, and electrical properties of $Ba_{0.85}Ca_{0.15}Ti_{0.90}Zr_{0.10}O_3$ lead-free ceramics were studied. A small amount of MnO_2 ($x \leq 0.25$) promotes the grain growth, improves the ferroelectricity and strengthens the tetragonal-orthorhombic phase transition near 40 °C. However, excess MnO_2 has an inhibition of grain growth, weakens the phase transition near 40 °C and thus degrades the ferroelectric and piezoelectric properties of the ceramics. Because of the coexistence of tetragonal and orthorhombic phases near room temperature and the combinatory effects of soft and hard doping of Mn ions, the d_{33}, k_p, and ε_r are enhanced considerably after 0.25 mol % MnO_2 doping. The ceramic with $x = 0.25$ exhibits the optimum piezoelectric properties ($d_{33} = 306$ pC/N and $k_p = 42.2$ %, respectively). The sintering temperature has an important influence on microstructure, tetragonal-orthorhombic phase

transition near 40 °C and electrical properties of the $Ba_{0.85}Ca_{0.15}Ti_{0.90}Zr_{0.10}O_3$ ceramics. The grain size is positively related with ferroelectric and piezoelectric properties. The ceramics with large grains possess more noticeable tetragonal–orthorhombic phase transition, stronger ferroelectricity and thus exhibits better piezoelectric properties than the ceramics with small grains. The $Ba_{0.85}Ca_{0.15}Ti_{0.90}Zr_{0.10}O_3$ ceramic sintered at 1350 °C possesses the high d_{33} value of 373 pC/N. The electrical properties and phase transition characters of the $Ba_{0.85}Ca_{0.15}Ti_{0.90}Zr_{0.10}O_3$ ceramics are very sensitive to sintering temperature and grain size.

Acknowledgements This study was supported by the projects of Education Department of Sichuan Province (11ZA104), Science and Technology Bureau of Sichuan Province (2010JQ0046) and the Open Projects of State Key Laboratory Cultivation Base for Nonmetal Composites and Functional Materials of Southwest University of Science and Technology (10zxfk27) and State Key Laboratory of Electronic Thin Films and Integrated Devices of University of Electronic Science and Technology of China (KFJJ201108).

References

1. Kuang SJ, Tang XG, Li LY, Jiang YP, Liu QX (2009) Scr Mater 61:68
2. Wei X, Wan X, Xi Y (2008) J Electroceram 21:226
3. Haertiling GH (1999) J Am Ceram Soc 82:797
4. Bechmann R (1956) J Acoust Soc Am 28:347
5. Liu W, Ren X (2009) Phys Rev Lett 103:257602
6. Li W, Xu Z, Chu R, Fu P, Zang G (2010) Mater Lett 64:2325
7. Zhang SW, Zhang HL, Zhang BP, Yang S (2010) J. Alloys Compd 506:131
8. Wu J, Xiao D, Wu W, Chen Q, Zhu J, Yang Z, Wang J (2011) Scr Mater 65:771
9. Li W, Xu Z, Chu R, Fu P, Zang G (2011) Mater Sci Eng, B 176:65
10. Wang P, Li Y, Lu Y (2011) J Eur Ceram Soc 31:2005
11. Wu J, Xiao D, Wu W, Zhu J, Wang J (2011) J Alloys Compd 509:L359
12. Su S, R. Zuo Z, Lu SB, Xu ZK, Wang XH, Li LT (2011) Curr Appl Phys 11:120–121
13. Li G, Zheng L, Yin Q (2005) J Appl Phys 98:064108
14. Hou Y, Zhu M, Gao F, Wang H, Wang B, Yan H, Tian C (2004) J Am Ceram Soc 87:847
15. Yu CS, Hsieh HL (2005) J Eur Ceram Soc 25:2425
16. Li SM, Lee SH, Yoon CB, Kim HE, Lee KW (2007) J Electroceram 18:311
17. Yan Y, Cho KH, Priya S (2011) J Am Ceram Soc 94:3953
18. Mgbemere HE, Herber RP, Schneider GA (2009) J Eur Ceram Soc 29:1729
19. Nagata H, Takenaka T (2001) J Eur Ceram Soc 21:1299
20. Fan X, Wang Y, Jiang Y (2011) J Alloys Compd 509:6652
21. Qiao L, Bi X (2009) J Eur Ceram Soc 29:1995
22. Buixaderas E, Bovtun V, Kempa M, Savinov M, Nuzhnyy D, Kadlec F, Vaněk P, Petzelt J, Eriksson M, Shen Z (2010) J Appl Phys 107:014111
23. Park Y, Lee WJ, Kim HG (1997) J Phys: Condens Matter 9:9445
24. Chattopadhyay S, Ayyub P, Palkar VR, Multani M (1995) Phys Rev B 52:13177
25. Damjanovic D, Demartin M (1997) J Phys: Condens Matter 9:4943
26. Zhang L, Zhong WL, Wang CL, Zhang PL, Wang YG (1998) Phys Stat Sol (a) 168:543
27. Martirenat HT, Burfoot JC (1974) J Phys C: Solid State Phys 7:1974
28. Cao W, Randall CA (1996) J Phys Chem Solids 57:1505
29. Randall CA, Kim N, Kucera JP, Cao W, Shrout TR (1998) J Am Ceram Soc 81:677
30. Demartin M, Damjanovic D (1996) Appl Phys Lett 68:3046
31. Damjanovic D (1998) Rep Prog Phys 61:1267